In situ self-assembling Au-DNA complexes for targeted cancer bioimaging and inhibition

Maonan Wang[a], Yun Chen[a], Weijuan Cai[a], Huan Feng[a], Tianyu Du[a], Weiwei Liu[a], Hui Jiang[a], Alberto Pasquarelli[b], Yossi Weizmann[c,1], and Xuemei Wang[a,1]

[a]State Key Laboratory of Bioelectronics (Chien-Shiung Wu Laboratory), School of Biological Science and Medical Engineering, Southeast University, 210096 Nanjing, China; [b]Institute of Electron Devices and Circuits, Ulm University, 89069 Ulm, Germany; and [c]Department of Chemistry, Ben-Gurion University of the Negev, 8410501 Beer-Sheva, Israel

Edited by Catherine J. Murphy, University of Illinois at Urbana–Champaign, Urbana, IL, and approved November 8, 2019 (received for review September 6, 2019)

Cancer remains one of the most challenging diseases to treat. For accurate cancer diagnosis and targeted therapy, it is important to assess the localization of the affected area of cancers. The general approaches for cancer diagnostics include pathological assessments and imaging. However, these methods only generally assess the tumor area. In this study, by taking advantage of the unique microenvironment of cancers, we effectively utilize in situ self-assembled biosynthetic fluorescent gold nanocluster-DNA (GNC-DNA) complexes to facilitate safe and targeted cancer theranostics. In in vitro and in vivo tumor models, our self-assembling biosynthetic approach allowed for precise bioimaging and inhibited cancer growth after one injection of DNA and gold precursors. These results demonstrate that in situ bioresponsive self-assembling GNC-PTEN (phosphatase and tensin homolog) complexes could be an effective noninvasive technique for accurate cancer bioimaging and treatment, thus providing a safe and promising cancer theranostics platform for cancer therapy.

biosynthetic complexes | self-assembling GNC-DNA complexes | cancer bioimaging and inhibition

Cancer is an extremely complex disease. Tumor cells can escape growth inhibition signals and programmed cell death and maintain their nutrient supply, all of which pose a great challenge to cancer therapy (1). Chemotherapy is currently the most widely used cancer treatment. Although traditional small-molecule chemotherapeutic drugs are widely used, these molecules have nonspecific tissue distribution, causing severe side effects such as myelosuppression (immunosuppression), gastrointestinal distress, alopecia, and organ damage (2). These negative effects contribute to patient suffering and can even lead to treatment failure. Therefore, the development of more effective treatments remains an area of active research.

In recent years, gene therapy has been considered an effective strategy for cancer treatment (3, 4). A large number of studies have found that targeting an increasing number of genes can inhibit angiogenesis, tumor growth, invasion, metastasis, and other critical features of cancer in vitro (5, 6). The phosphatase and tensin homolog (*PTEN*) gene is one of the most well-studied tumor suppressor genes, and mutations in this gene occur at high frequency in numerous tumor types. Reduced *PTEN* expression contributes to the difficulty in cancer treatment (7, 8). Numerous studies have also shown that increasing *PTEN* expression in the tumor can inhibit the proliferation, invasion, metastasis, and other critical oncogenic characteristics of tumor cells (9, 10). Plasmid DNA-based gene therapy has recently shown enhanced permeability and retention and has led to the accumulation of passive drugs in tumor tissues (11). The combination of gene therapy and chemotherapy can improve treatment success rates of cancer patients. However, it is usually following treatment that the therapeutic effect can be visualized using CT, ultrasound, or magnetic resonance imaging. These diagnosis and treatment methods are difficult to evaluate the development of the tumors in real time. This can lead to decision-making failures and lower treatment success rates, especially with surgery. Therefore, it is essential to improve treatment success rates of cancer therapy and to discover a therapeutic that can also help monitor tumor growth in real time. This dual effect of a compound would enable the integration of diagnostics and therapeutics.

The use of nanotechnology and biocompatible nanomaterials to facilitate cancer diagnostics and treatments has recently been a focus on the cancer field. Among the various types of biocompatible nanomaterials (12–15), gold nanoclusters (GNCs) have recently been utilized in bioimaging and other biomedical applications because of the favorable intrinsic optical characteristics, highly stable chemical properties, and good biocompatibility (16–19). Based on the advantages of in situ bioresponsive biosynthetic gold nanoclusters in fluorescent imaging and therapy (20), we proposed the use of in situ self-assembled biosynthetic fluorescent gold nanocluster-DNA (GNC-DNA) complexes to facilitate accurate cancer bioimaging and targeted treatment.

In this study, we explored the possibility of utilizing in situ bioresponsive self-assembled fluorescent GNC-DNA complexes through a biosynthetic strategy that takes advantage of the unique tumor microenvironment. Fig. 1 illustrates the strategy for safe and targeted cancer theranostics. Furthermore, by forming a complex with DNA from the tumor suppressor *PTEN*, we observed that in situ bioresponsive self-assembled complexes could readily label

Significance

Although many efforts have been devoted to localize and monitor cancer progression, it is still difficult to precisely evaluate the development of cancers for efficient targeted treatments. Herein, we demonstrate a straightforward strategy using in situ self-assembly of gold nanocluster–DNA complexes. In combination with the tumor suppressor gene-phosphatase and tensin homolog (PTEN), the gold nanocluster-PTEN complexes could realize targeted bioimaging and identification of cancers and simultaneously inhibit the effect of relevant oncogenes. Meanwhile, these biocompatible self-assembling gold nanocluster–PTEN complexes cannot only facilitate safe and targeted therapeutics, but can also avoid the side effects of conventional DNA transfection. This strategy allows the possibility of establishing a multimode platform for accurately targeted cancer theranostics to eradicate tumors and vascularized metastases.

Author contributions: M.W., Y.C., Y.W., and X.W. designed research; M.W., Y.C., W.C., T.D., W.L., and H.J. performed research; W.C., H.F., and T.D. contributed new reagents/analytic tools; Y.C., W.L., H.J., Y.W., and X.W. analyzed data; and M.W., A.P., Y.W., and X.W. wrote the paper.

The authors declare no competing interest.

This article is a PNAS Direct Submission.

[1]To whom correspondence may be addressed. Email: yweizmann@bgu.ac.il or xuewang@seu.edu.cn.

This article contains supporting information online at https://www.pnas.org/lookup/suppl/doi:10.1073/pnas.1915512116/-/DCSupplemental.

First published December 16, 2019.

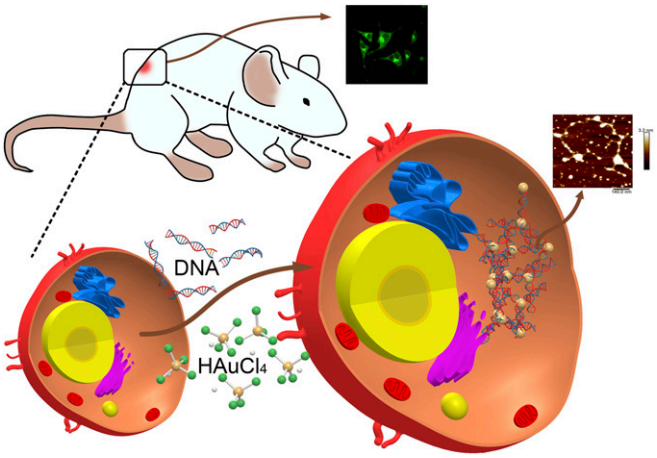

Fig. 1. Schematic diagram of in situ self-assembled biosynthetic GNC-DNA complexes in cancer cells.

and inhibit tumor growth both in vitro and in vivo. Therefore, our study demonstrates a practical approach to integrating effective cancer diagnostics and therapeutics through in situ bioresponsive self-assembled GNC-DNA, providing a safe and efficacious theranostics approach for cancer therapeutics.

Results and Discussion

Characterization of Self-Assembled GNC-DNA Complexes. The specific tumor microenvironment (19, 20) is usually exploited by in situ imaging because of the presence of relatively high amounts of molecules that act as reducing agents for GNC syntheses, such as reactive oxygen species (ROS), L-glutathione, and NADPH (21–23). In the present study, we utilized natural double-stranded DNA (dsDNA) from herring sperm (<50 bp) to explore the usage of bioresponsive self-assembled biosynthetic GNC-DNA fluorescent complexes in cancer. Based on a previously published study (19), we used a suitable concentration of gold precursor solution (20 μM pH = 7.2) without evident cytotoxicity in HeLa (cervical carcinoma), A549 (lung cancer), and L02 (normal hepatocyte) cells (*SI Appendix*, Fig. S1).

To confirm the formation of GNC-DNA complexes, we harvested cytoplasmic DNA from cells and further characterized this DNA by atomic force microscopy (AFM), transmission electron microscope (TEM), X-ray photoelectric spectroscopy (XPS), and other spectroscopies. Fig. 2 *A–C* and *SI Appendix*, Fig. S2 *A–F* demonstrate the in situ bioresponsive self-assembled biosynthetic GNC-DNA complexes isolated from cancer cells that had been incubated with DNA and gold precursors. No complexes were observed in cells cultured only with the gold precursor solution. The highest of the sample was just 1.3 nm (*SI Appendix*, Fig. S3). From the AFM height profiles (Fig. 2 *D–F*), it is evident that the cumulative height of GNC-DNA appears to be approximately 4 nm, while the double-stranded DNA helix diameter is estimated to be 2 nm. These observations indicate that the height of GNCs is 2 nm. This size is consistent with the TEM characterization (*SI Appendix*, Fig. S2 *G* and *H*).

We used surface-enhanced Raman spectroscopy (SERS) (Fig. 2*G*) and Fourier transforms infrared spectra (FTIR) (Fig. 2*H*) to investigate the interaction between the GNCs and DNA in the self-assembly GNC-DNA complexes (24–28). As illustrated by the FTIR spectra, there were no noticeable differences between the presence of GNC-DNA complexes and DNA alone. Therefore, it appears that the attachment of GNCs has little effect on the deoxyribose and the base groups of DNA. In comparison, the SERS spectra showed that a roughly 16-fold Raman signal enhancement occurred after the formation of GNC-DNA complexes. The typical DNA vibration peaks could be clearly recognized using SERS. The GNC-DNA complexes could effectively enhance the relevant DNA vibration peaks using Raman spectroscopy. In addition, purine respiratory vibration, the DNA deoxyribose backbone, and N-H stretching vibration could be observed in the related SERS spectra (*SI Appendix*, Table S1). The existence of GNCs caused the deformation and stretching of DNA, which further indicates the specific interaction between DNA and GNCs to form GNC-DNA complexes.

We also measured the emission fluorescence of the extracted GNC-DNA complexes by measuring emission peaks at 566 and 710 nm after excitation with 470 nm (Fig. 2*I*). Laser confocal fluorescent microscopy (Fig. 2*J*) demonstrated that both HeLa and A549 cells cultured with gold precursors and DNA had much stronger intracellular fluorescence when compared with that of the groups cultured only with gold precursors. This observation suggests that this complex can enhance intracellular fluorescence. In contrast, such fluorescent characteristics were not observed in normal cells under identical experimental conditions. This supports that there was specific formation of bioresponsive GNC-DNA complexes in vivo that specifically form in the distinct cancer microenvironment (29, 30). These complexes can also be used as simple but effective self-assembling nanoscale biomarkers for targeted cancer cell imaging.

Inhibition of Cancer Development in Vitro Using in Situ Self-Assembly of GNC-PTEN Complexes. Gene-targeted therapy for cancer has attracted much attention recently, with circular plasmids being used to improve the expression efficiency of target DNA (31). Nanoclusters are also emerging as a vehicle for accurate gene delivering to the tumor site. Early clinical results suggest that the specific tumor targeting and active cellular uptake of nanotherapy can improve therapeutic efficacy (32). An enhanced targeting to the tumor tissue can also be accomplished by improving pharmacokinetics and pharmacodynamics and utilizing positive intracellular delivery (33, 34). We have further explored the possibility of enhancing cancer treatment efficacy by using in situ bioresponsive self-assembling biosynthetic GNC-PTEN complexes. Specifically, our studies utilize the tumor suppressor gene *PTEN* to form the complexes. *PTEN* is a tumor suppressor frequently mutated in various tumor types (35, 36). The protein encoded by this gene is a phosphatidylinositol-3,4,5-trisphosphate 3-phosphatase. After inserting the coding sequence of *PTEN* into the universal pmCherry-N1 vector, we obtained the double-stranded *PTEN* overexpression vector (*SI Appendix*, Fig. S4). The concentration of *PTEN* DNA was chosen based on the minimum amount needed in the previous dsDNA experiment. After adding *PTEN* DNA (2 ng/μL) and gold precursors (20 μM) to the cell suspension for 4 h, we washed the cells with deionized water 3× and broke up the cell suspension to obtain GNC-PTEN complexes.

AFM (*SI Appendix*, Fig. S5) and TEM images (Fig. 3 *A–C*), as well as fluorescent characterization (Fig. 3*D*) of these complexes, provide consistent evidence of self-assembling GNC-PTEN complexes made with herring sperm DNA. The SERS (Fig. 3*E*) and FTIR spectra (Fig. 3*F*) of the extracted GNC-PTEN complexes also demonstrate that the phosphodiester bond of DNA was distorted and deformed. This indicates the interaction between the relevant group of *PTEN* DNA and bioresponsive GNCs, which is similar to what was observed with self-assembling GNC-PTEN complexes (*SI Appendix*, Fig. S6). Furthermore, we carried out an XPS study to confirm the binding of *PTEN* DNA to GNCs in the atomic composition (*SI Appendix*, Fig. S7). After the successful formation of the complex between *PTEN* DNA and GNCs, the amount of gold on the surface decreased, while the amount of carbon, nitrogen, and oxygen were slightly higher than that in GNCs. The decrease in gold may be due to the presence of a large amount of DNA on the surface of the complex, which would reduce the amount of gold exposed to

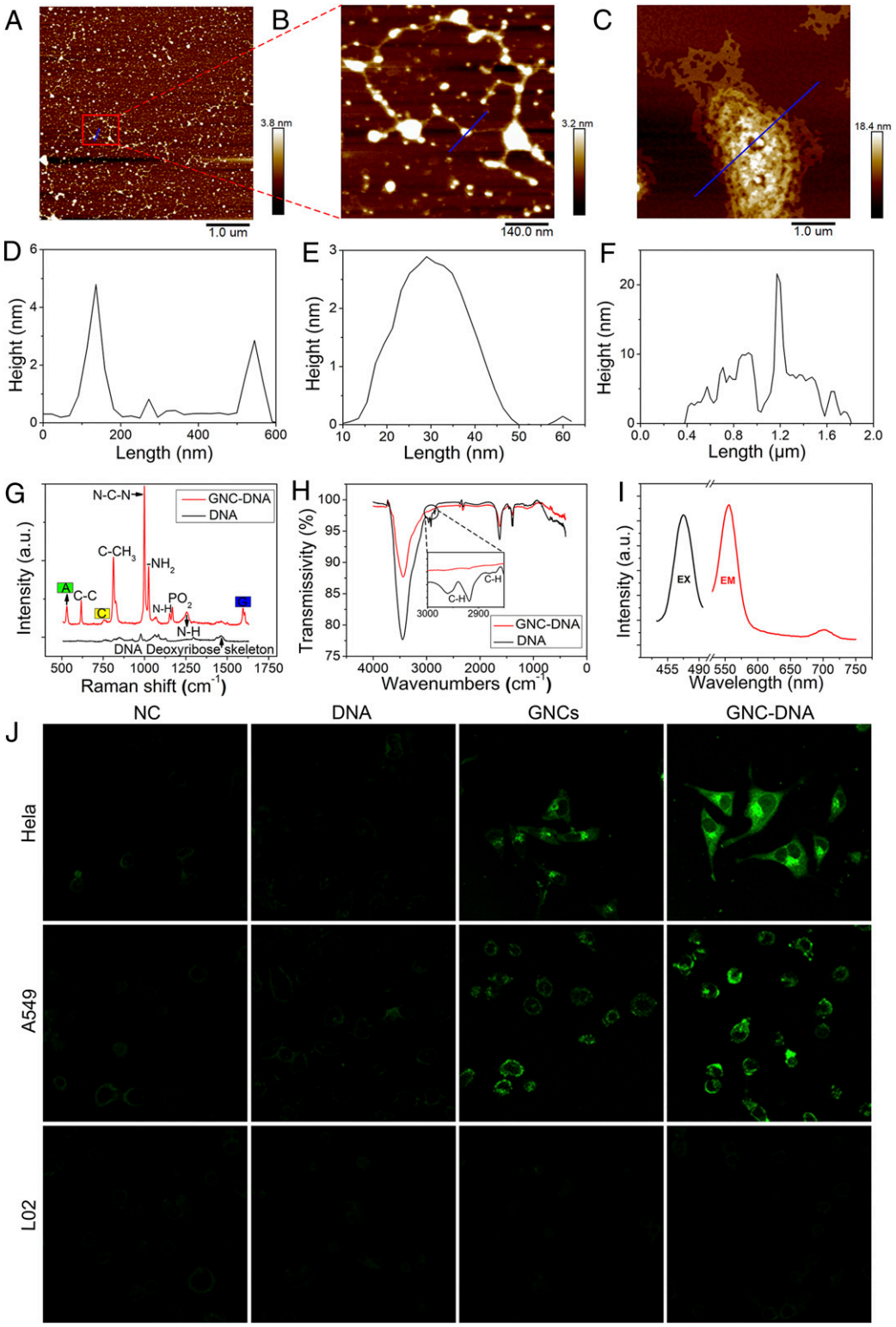

Fig. 2. AFM images of the bioresponsive self-assembled biosynthetic GNC-DNA complexes in cancer cells. (*A*) Typical AFM image of the biosynthetic GNC-DNA complexes extracted from HeLa cells when cultured with gold precursors (20 μM) and DNA solution (2 ng/μL). (*B*) Enlarged image from a location in *A*. (*C*) Typical AFM image of the extracted biosynthetic GNC-DNA complexes obtained with the gold precursor solution (20 μM) and a relatively high concentration of DNA solution (0.1 mg/μL). (*D–F*) Height maps at the blue line segment in *A–C*, respectively. (*G*) Raman spectra and (*H*) FTIR spectra of the different experimental groups. a.u., arbitrary unit; A, adenine; C, cytosine; G, guanine. (*I*) Fluorescence spectra of the complexes. EX, excitation wavelength; EM, emission wavelength. (*J*) Laser confocal fluorescence images of a series of cells cultured with DMEM, DNA, gold precursors, and both DNA and gold precursors, respectively. When excited at 488 nm, the relatively stronger intracellular fluorescence of the biosynthesized GNC-DNA complexes was observed compared with the corresponding control cancer cells with the biosynthesized GNCs alone or with the normal cell (L02) that did not have intracellular fluorescence in any experimental condition. In the above tests, the concentration of DNA was 2 ng/μL, while the gold precursor solution was 20 μM.

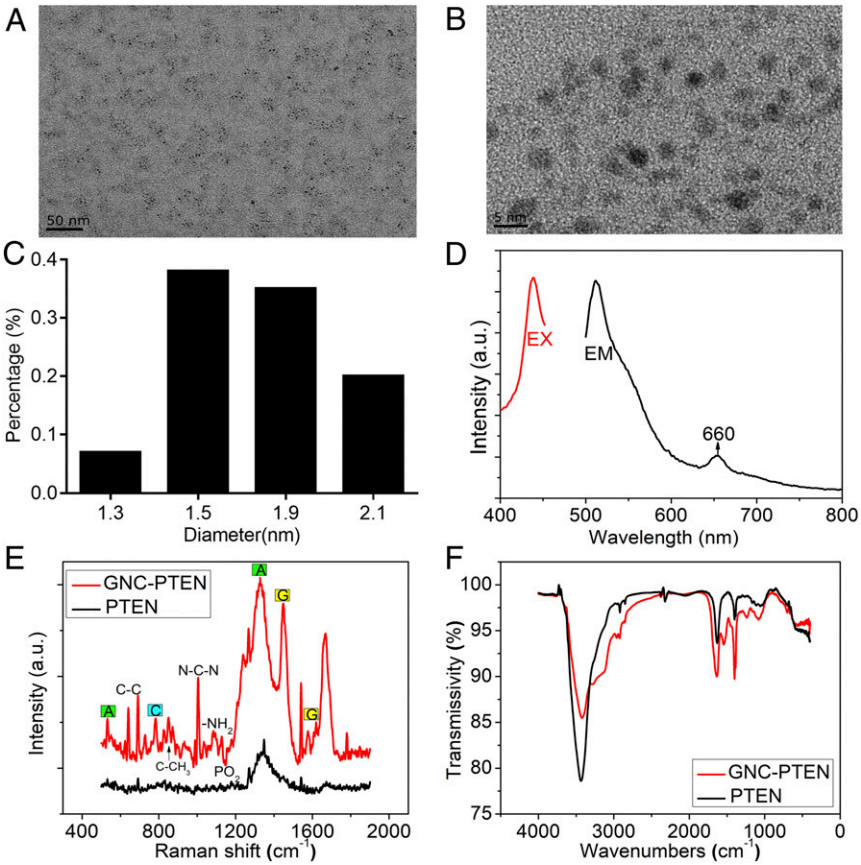

Fig. 3. Self-assembled GNC-PTEN complex characteristics. Typical (*A*) TEM and (*B*) High resolution (HR)-TEM image of the isolated GNC-PTEN complexes. (*C*) The particle-size distribution of gold nanoparticles. (*D*) Fluorescence spectra of the aqueous solution of the extracted GNC-PTEN complexes show that the relevant emission peak wavelengths were 515 and 660 nm, respectively, when the excitation wavelength (EX) was 445 nm. EM, emission wavelength. (*E*) Raman spectra of the extracted GNC-PTEN complexes and *PTEN* DNA alone. (*F*) FTIR spectra of the abstracted GNC-PTEN complexes and *PTEN* DNA alone. For the control group (black), only *PTEN* DNA alone was added. Red curve shows the results of the in situ synthesized *PTEN* GNC-DNA. a.u., arbitrary unit.

the surface. This can also explain the increase in carbon, nitrogen, and oxygen on the surface of the complex. However, phosphorus was increased in the complex, which may be due to the large number of nucleotides and phosphates in DNA. The precipitation of DNA leads to the slight increase in phosphorus in this complex. The above experiments directly support the successful formation of GNC-PTEN complexes.

By using RT-PCR and western blotting, we found that the biosynthetic GNC-PTEN complexes yielded higher *PTEN* messenger RNA (mRNA) and protein-level expression (Fig. 4*A*). It was expected that the overexpression of *PTEN* could significantly inhibit the growth and development of tumor cells. Moreover, we further examined the effect of *PTEN* overexpression on proliferation, migration, and metastasis of tumor cells. It is worth noting that, compared with the negative control group, the proliferation of A549 and HeLa cells with biosynthesized GNC-PTEN complexes was significantly decreased (Fig. 4*B*). These observations demonstrate that these bioresponsive self-assembling biosynthetic GNC-PTEN complexes could inhibit the proliferation of cancer cells. In scratch-healing and transwell invasion experiments, we found that the migration and invasion of A549 and HeLa cells in the presence of GNC-PTEN complexes were significantly decreased, which indicated that these complexes could effectively inhibit the migration and invasion of tumor cells (Fig. 4 *C* and *D*).

Based on these studies, we further investigated ROS levels in A549 and HeLa cells in different treatment groups. The results show that intracellular ROS levels in relevant cancer cells in the presence of GNC-PTEN complexes were significantly higher than that in the control groups (Fig. 4*E*). It has already been reported in the literature that the significant increase of ROS can induce apoptosis and even kill tumor cells (37–39). These results further suggest that bioresponsive self-assembling biosynthetic GNC-PTEN complexes can effectively inhibit the oncogenic characteristics of tumor cells, such as proliferation, invasion, metastasis, and promote apoptosis. This, combined with targeted fluorescent bioimaging, demonstrates that the in situ bioresponsive self-assembled biosynthetic complexes provide a promising prospect in targeted tumor theranostics.

In Situ Self-Assembling GNC-PTEN Complexes in Cancer Bioimaging and In Vivo Cancer Growth Inhibition. To better understand and simulate the therapeutic effect of the in situ synthesized GNC-PTEN complexes in vivo, we established a s.c. tumor mouse model (*SI Appendix*, Fig. S8) and randomly divided mice into 4 groups, with 4 mice per group. Mice were injected with either the gold precursor solution (0.3 mmol) and *PTEN* DNA solution (40 μg), gold precursor solution (0.3 mmol) alone, *PTEN* DNA solution (40 μg) alone, or an equal volume of normal saline. After the 5th injection, 1 mouse in each group was randomly selected for in vivo fluorescent imaging to examine tumor localization of in situ synthesized complexes within 24 h (Fig. 5*A*).

Fluorescent intensity in the tumor tissue at different periods is shown in Fig. 5*B*. Compared with free *PTEN* DNA and the saline control group, GNC-PTEN complexes showed increased aggregation in the tumor. The fluorescent signal was also stronger in the

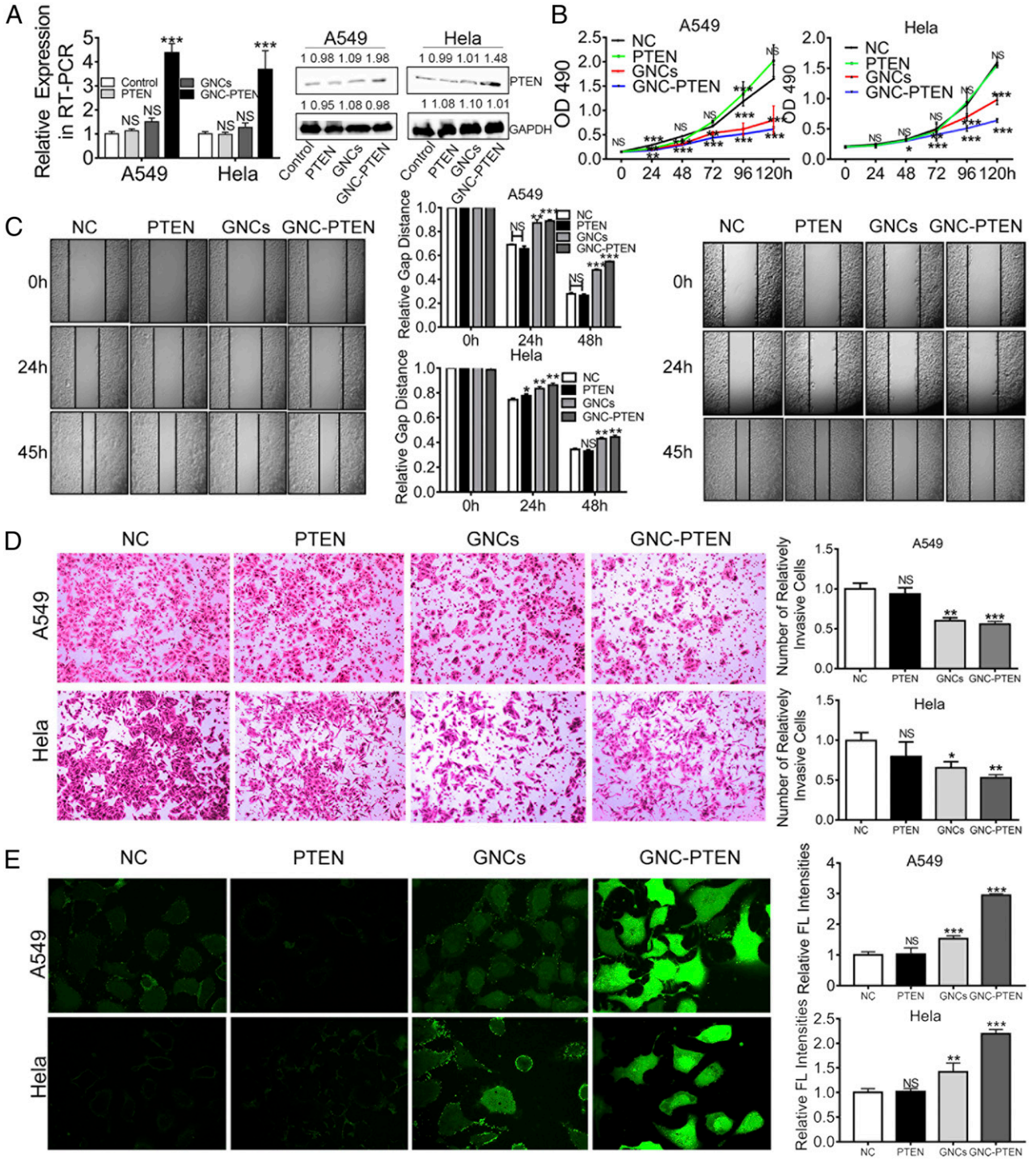

Fig. 4. In situ self-assembled biosynthetic GNC-PTEN complexes inhibit tumor cell growth. (*A*) Measurement of *PTEN* mRNA (RT-PCR) and protein levels (Western blot) from the different groups. The first line on the right is PTEN protein expression, and the second line is GAPDH protein expression. (*B*) MTT proliferation assay of A549 cells and HeLa cells under different conditions. The black, green, red, and blue lines represent the negative control group, PTEN group (PTEN, 2 ng/μL), in situ synthetized GNCs (gold precursor, 20 μM), and in situ GNC-PTEN complex group (PTEN, 2 ng/μL; gold precursor, 20 μM), respectively. (*C*) Images of a scratch-healing experiment with A549 and HeLa cells, respectively. Statistical results are between the two images. (*D*) Representative images of a transwell invasion experiment with A549 and HeLa cells. Images on the right show statistical results in the same group. *C* and *D* were taken using an inverted microscope (100×). (*E*) The ROS of different treatment groups. Fluorescent intensity indicates the strength of ROS in A549 and HeLa cells. Each image was taken using a laser confocal microscope (600×). The image on the right shows the fluorescent (FL) intensity of the different treatment groups and the fluorescent value measured by the enzyme-labeling instrument. ***$P < 0.001$; **$P < 0.01$; *$P < 0.05$; NS, no significant difference.

GNC-PTEN complex group than that in the GNC group. The in vivo fluorescent signals indicated that after 6 h, exogenous DNA and gold precursors accumulated and self-assembled into GNC-PTEN complexes at the tumor site. Twenty-four hours after injection, ex vivo fluorescent imaging showed that tumors treated with GNC-PTEN complexes exhibited a higher level of fluorescence intensity

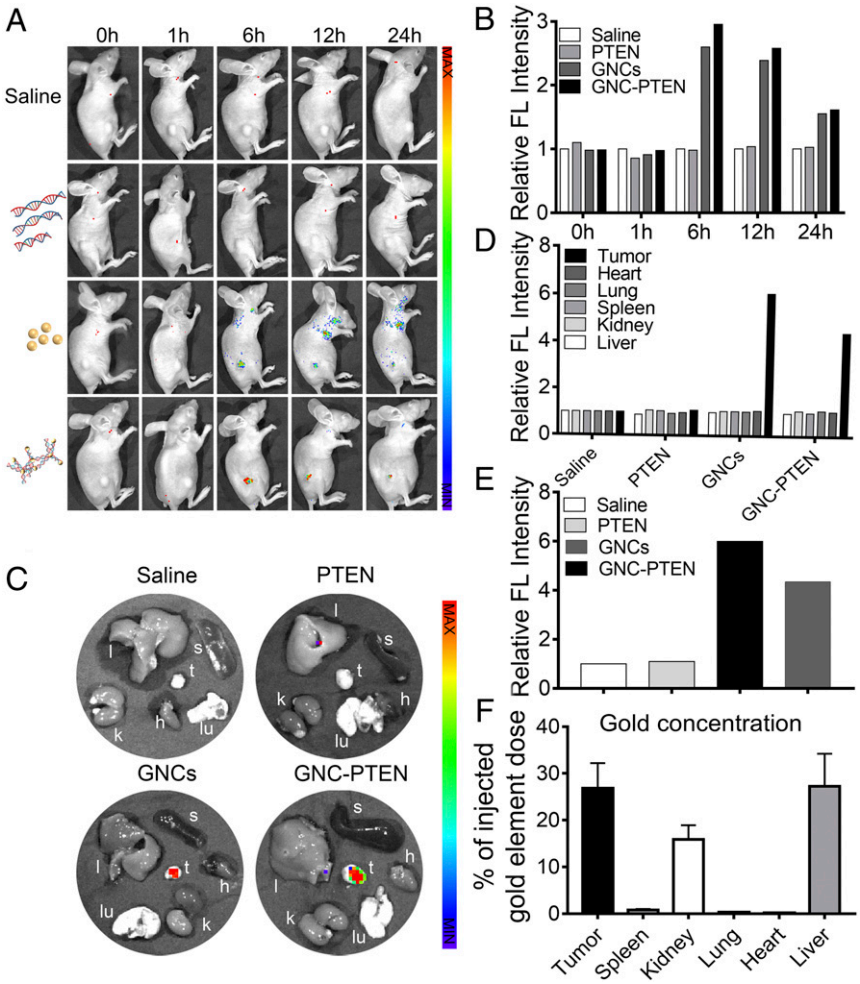

Fig. 5. Bioimaging of tumors in vivo using self-assembled biosynthesized GNC-PTEN complexes. (*A*) Dynamic biodistribution of normal saline, PTEN, GNC, and GNC-PTEN complexes in mice using fluorescent imaging at 0, 1, 6, 12, and 24 h (excitation wavelength: 420 nm, emission wavelength: 620 nm). (*B*) Quantitative analysis of the relative fluorescent light intensity. The fluorescent intensity of the control group was standardized to 1. (*C*) Twenty-four hours after injection, animals were killed and tumor (t, tumor) as well as major organs (l, liver; k, kidney; s, spleen; lu, lung; and h, heart) were collected for ex vivo imaging. (*D*) Fluorescent intensity of tumors in 4 groups. (*E*) Fluorescent intensity of individual organs in different treatment groups. The fluorescent intensity of the control group was standardized to 1. The fluorescent intensities of tumors are shown separately. (*F*) Inductively plasma mass spectrometer(ICP-MS) analysis of gold element in different organs of mice of the GNC-PTEN group after ex vivo imaging.

than the other groups (Fig. 5 *C*–*E*). Inductively coupled plasma mass spectrometry confirmed that the amount of gold in GNC-PTEN complexes accumulated in the tumor site (Fig. 5*F*). Gold was mainly eliminated in vivo by the liver and kidneys, which is consistent with previous reports (40, 41).

The resulting fluorescence intensified in tumors, indicating that the in situ biosynthesized fluorescent GNC-PTEN complexes were present in target tumors. Consistent with the observations obtained from in vitro experiments, the bioresponsive self-assembled biosynthetic GNC-PTEN complexes showed enhanced inhibition of tumor growth. The antitumor effects observed in the remaining 3 mice per each group demonstrated significant therapeutic efficacy. In vivo fluorescent imaging is shown in Fig. 6*A*, and ex vivo imaging of each mouse is shown in Fig. 6*B*. Compared with the control and the *PTEN* DNA group, the growth of tumors in the in situ biosynthesized GNC-PTEN complex group decreased significantly, with some tumors considerably shrinking. Conversely, the group with in situ biosynthetic GNCs alone showed a slight decrease (Fig. 6*C*). Statistics of tumor size and weight are included in Fig. 6 *D* and *E*. No significant changes in mouse weights were observed during treatment (Fig. 6*F*), and hematoxylin-eosin staining of the main organs (*SI Appendix*, Fig. S9) indicated that there were no obvious toxicities caused by the in situ biosynthesized GNC-PTEN complexes.

To further evaluate the safety of the complexes in vivo, we measured biochemical parameters in the blood (*SI Appendix*, Table S2) after killing mice. The results showed that there were no significant differences in erythrocytes, leukocytes, or platelets between mice in the experimental groups and the 3 control groups. In addition, aspartate transaminase, alanine transaminase, blood urea nitrogen, and purine trione measurements showed that the self-assembled biosynthetic GNC-PTEN complexes did not cause damage to liver and kidneys in mice (*SI Appendix*, Table S3). This indicates that the complexes pose a low risk of serious side effects in normal organs and tissues. These results reconfirmed our hypothesis that the in situ biosynthesized GNC-PTEN complexes could effectively inhibit tumor progression without significant toxicities. This is consistent with the in vitro results. These observations suggest that the GNC-PTEN complexes have good tumor targeting and therapeutic effects, which can be used to integrate targeted treatment and tumor diagnostics. Overall, it is evident that the in situ synthesized GNC-PTEN complexes are safe with low toxicity. This could provide an intelligent strategy and promising candidate for advanced theranostics platforms for highly effective cancer therapy.

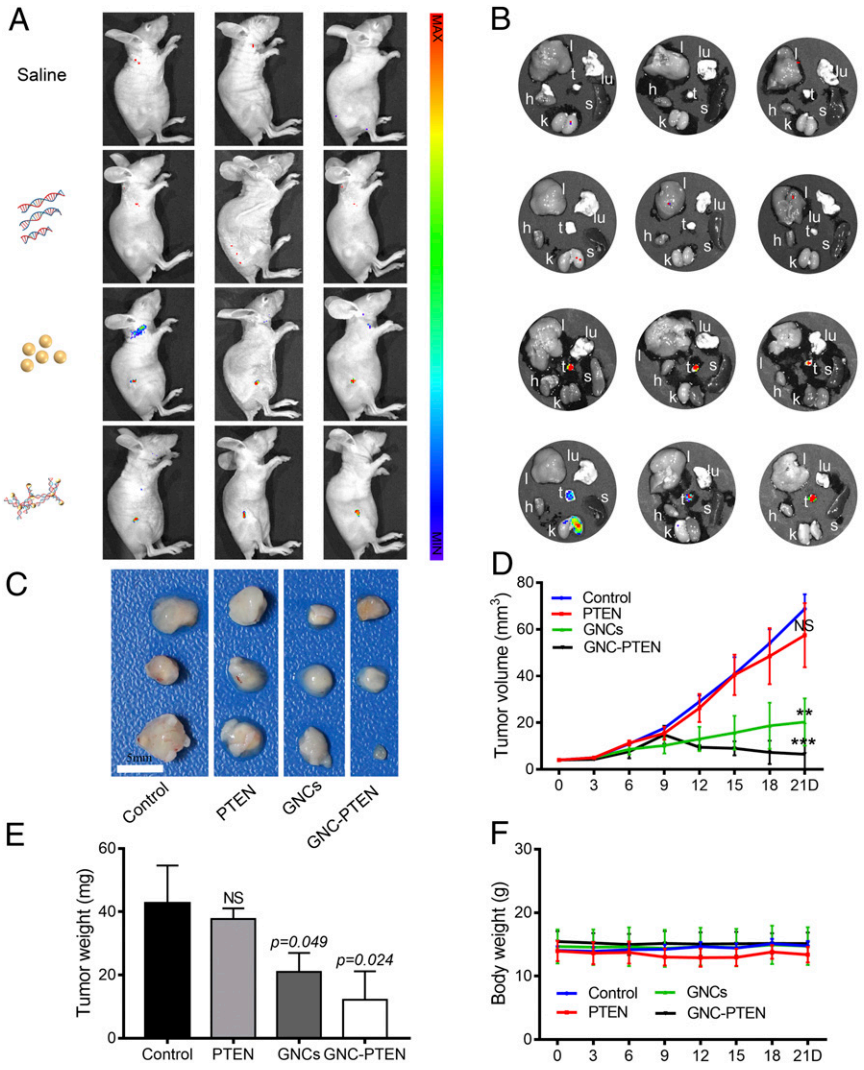

Fig. 6. The antitumor effects of the GNC-PTEN complexes in s.c. tumors. (*A*) Fluorescent images 12 h after the last injection in the 4 groups of mice [excitation wavelength (ex): 420 nm, emission wavelength (em): 620 nm]. From top to bottom: control, PTEN, GNC, and GNC-PTEN complex groups. (*B*) Ex vivo imaging of major organs (l, liver; k, kidney; s, spleen; lu, lung; and h, heart) and tumors (t, tumors) in corresponding photograph of each mouse shown in *A* (ex: 420 nm, em: 620 nm). (*C*) Tumor images on day 21. (Scale bar, 5 mm.) (*D*) Tumor sizes measured within 21 d. Compared with the control group, the significant difference in the last measurement of the 3 groups is marked in the figure. (*E*) Weight of the isolated tumors. (*F*) Weight of each group of mice. NS, no significant difference. $^{**}P < 0.01$, $^{***}P < 0.001$.

Mechanism of Tumor Growth Inhibition with Self-Assembled GNC-PTEN Complexes. To further explore the molecular mechanism of tumor growth inhibition with self-assembled GNC-PTEN complexes, we performed RNA-seq analysis of HeLa cells in different treatment groups, a blank control group, and a *PTEN* DNA and gold precursor group. The results showed that the mRNA level of a large number of genes changed in the in situ synthesized GNC-PTEN complex group compared with the control group. Significantly up-regulated genes in the GNC-PTEN group were defined as having gene expression 3 times higher than that in the control group, and down-regulated gene expression was defined as having expression lower than 0.33 that of the control group (Fig. 7 *A* and *B*).

There were 83 genes up-regulated and 59 genes down-regulated in the bioresponsive self-assembled biosynthetic GNC-PTEN complex group. In addition, compared with the control group, the up-regulation of tumor-suppressor genes and the down-regulation of oncogenes was greater in the bioresponsive self-assembled biosynthetic GNC-PTEN complex group. In addition to *PTEN*, tumor suppressor genes *OSGIN1* (42), *PARP3* (43), *SAMD9L* (44), and *TP53* (45), among others, were up-regulated significantly, while oncogenes such as *IL33* (46), *F2RL1* (47), *MT2A* (48), *IL8* (49), and *STX2* (50) were down-regulated in the bioresponsive GNC-PTEN complex group (Fig. 7*C*). This further demonstrates that the DNA complex can inhibit tumor development, perhaps by changing the expression of oncogenes and tumor suppressor genes.

In summary, we have demonstrated that the formation of in situ bioresponsive self-assembling biosynthetic GNC-DNA complexes could be readily realized in the cancer setting for simultaneously targeting bioimaging and effective theranostics. In addition, utilizing *PTEN* DNA could allow for usage of bioresponsive self-assembled biosynthetic fluorescent GNC-PTEN complexes for real-time targeted bioimaging and inhibition of tumor growth. Furthermore, we found that the biosynthesized complexes can effectively inhibit tumor development through up-regulation of tumor suppressor genes and down-regulation of oncogenes. These GNC-PTEN complexes can facilitate targeted diagnostics and therapeutic effects, and in addition, they also have few side effects and biological toxicities normally associated with traditional DNA transfection. Thus, the strategy of the in situ bioresponsive self-assembling of biosynthetic GNC-DNA complexes holds great

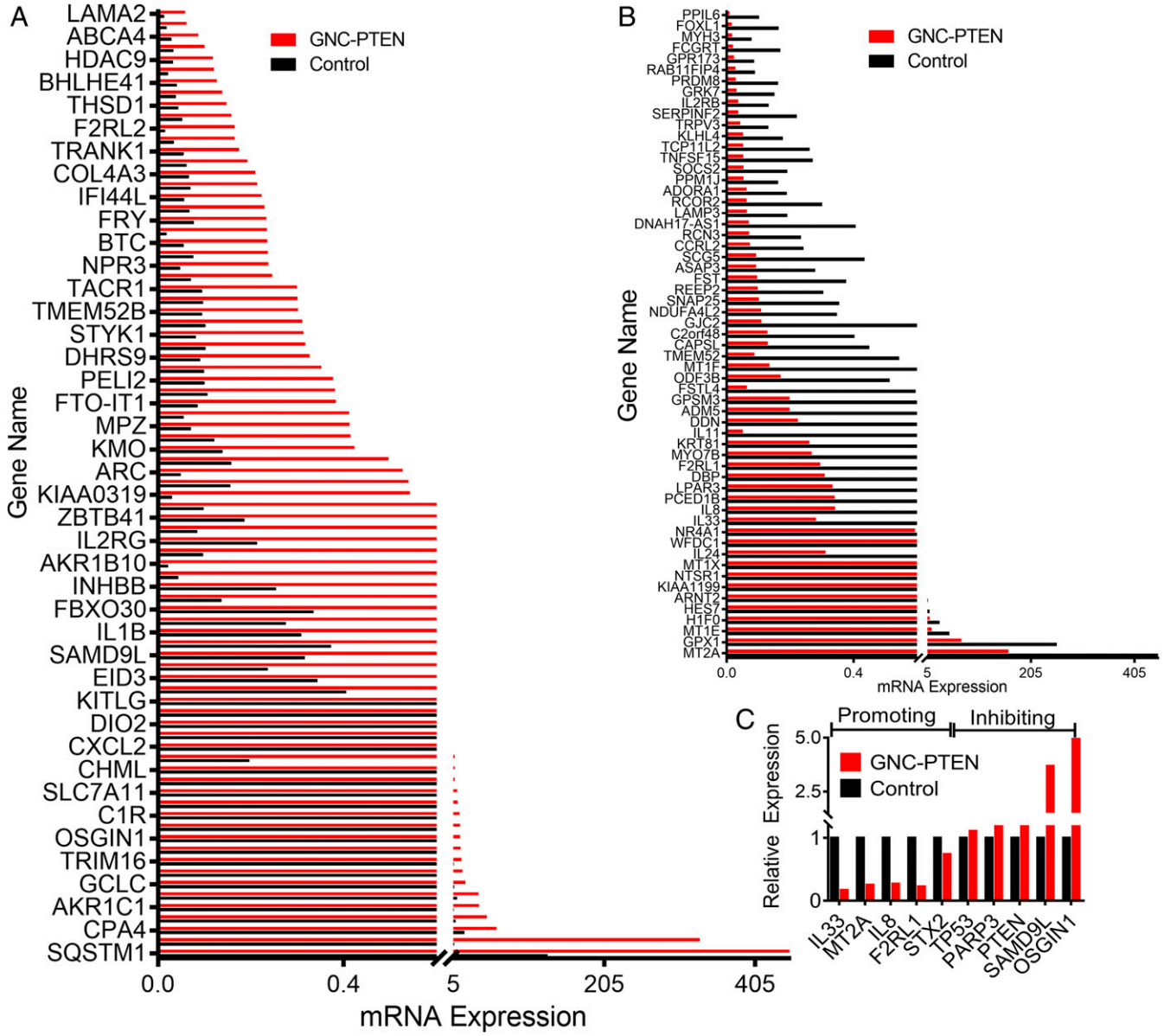

Fig. 7. Differential expression of mRNA levels in the self-assembled GNC-PTEN complex group compared with the control group. (*A*) Up-regulated and (*B*) down-regulated genes in the GNC-PTEN complex group. (*C*) Oncogene and tumor suppressor gene expression in the self-assembled GNC-PTEN complex group compared with the control group. The expression of the control group was standardized to 1.

promise for integrating simultaneous diagnostics and treatment. This raises the possibility of establishing a multimodal platform for targeted cancer theranostics to eradicate tumors and metastases.

Materials and Methods

The materials and methods used in this study are described in detail in *SI Appendix*. Information includes preparation of in situ biosynthetic GNC-DNA complexes, characteristic imaging analysis, in vitro cell experiments, in vivo animal experiments, and molecular biology experiments. All experiments involving mice were approved by the National Institute of Biological Science and Animal Care Research Advisory Committee of Southeast University, and the experiments were conducted by following the guidelines of the Animal Research Ethics Board of Southeast University.

Data Availability. All data generated or used during the study appear in the submitted article.

ACKNOWLEDGMENTS. This work was supported by the National Natural Science Foundation of China (91753106, 21675023, and 81325011), the National Key Research and Development Program of China (2017YFA0205300), and Primary Research and Development Plan of Jiangsu Province (BE2019716).

1. D. Hanahan, R. A. Weinberg, Hallmarks of cancer: The next generation. *Cell* **144**, 646–674 (2011).
2. B. A. Chabner, T. G. Roberts, Jr, Timeline: Chemotherapy and the war on cancer. *Nat. Rev. Cancer* **5**, 65–72 (2005).
3. M. Morille, C. Passirani, A. Vonarbourg, A. Clavreul, J. P. Benoit, Progress in developing cationic vectors for non-viral systemic gene therapy against cancer. *Biomaterials* **29**, 3477–3496 (2008).
4. D. Wang *et al.*, Bottlebrush-architectured poly(ethylene glycol) as an efficient vector for RNA interference in vivo. *Sci. Adv.* **5**, eaav9322 (2019).
5. M. H. Kershaw, J. A. Westwood, P. K. Darcy, Gene-engineered T cells for cancer therapy. *Nat. Rev. Cancer* **13**, 525–541 (2013).
6. M. Cavazzana, F. D. Bushman, A. Miccio, I. André-Schmutz, E. Six, Gene therapy targeting haematopoietic stem cells for inherited diseases: Progress and challenges. *Nat. Rev. Drug Discov.* **18**, 447–462 (2019).

7. H. Xia, L. L. P. J. Ooi, K. M. Hui, MicroRNA-216a/217-induced epithelial-mesenchymal transition targets PTEN and SMAD7 to promote drug resistance and recurrence of liver cancer. *Hepatology* **58**, 629–641 (2013).
8. K. A. Leinonen *et al*., Loss of PTEN is associated with aggressive behavior in ERG-positive prostate cancer. *Cancer Epidemiol. Biomarkers Prev.* **22**, 2333–2344 (2013).
9. X. Yan, M. Fraser, Q. Qiu, B. K. Tsang, Over-expression of PTEN sensitizes human ovarian cancer cells to cisplatin-induced apoptosis in a p53-dependent manner. *Gynecol. Oncol.* **102**, 348–355 (2006).
10. M. K. Park *et al*., PTEN self-regulates through USP11 via the PI3K-FOXO pathway to stabilize tumor suppression. *Nat. Commun.* **10**, 636–652 (2019).
11. D. Jiang *et al*., DNA origami nanostructures can exhibit preferential renal uptake and alleviate acute kidney injury. *Nat. Biomed. Eng.* **2**, 865–877 (2018).
12. J. Li, A. A. Green, H. Yan, C. Fan, Engineering nucleic acid structures for programmable molecular circuitry and intracellular biocomputation. *Nat. Chem.* **9**, 1056–1067 (2017).
13. K. Lee *et al*., Nanoparticle delivery of Cas9 ribonucleoprotein and donor DNA *in vivo* induces homology-directed DNA repair. *Nat. Biomed. Eng.* **1**, 889–901 (2017).
14. B. Lee *et al*., Nanoparticle delivery of CRISPR into the brain rescues a mouse model of fragile X syndrome from exaggerated repetitive behaviours. *Nat. Biomed. Eng.* **2**, 497–507 (2018).
15. K. Ni *et al*., Nanoscale metal-Organic framework mediates radical therapy to enhance cancer immunotherapy. *Chem* **5**, 1892–1913 (2019).
16. L. Y. Chen, C. W. Wang, Z. Yuan, H. T. Chang, Fluorescent gold nanoclusters: Recent advances in sensing and imaging. *Anal. Chem.* **87**, 216–229 (2015).
17. S. Atta, A. M. Pennington, F. E. Celik, L. Fabris, TiO2 on gold nanostars enhances photocatalytic water reduction in the near-infrared regime. *Chem* **4**, 2140–2153 (2018).
18. J. Sharma *et al*., Control of self-assembly of DNA tubules through integration of gold nanoparticles. *Science* **323**, 112–116 (2009).
19. M. Lian *et al*., Movable hollow nanoparticles as reactive oxygen scavengers. *Chem* **5**, 2378–2387 (2019).
20. J. Wang *et al*., In vivo self-bio-imaging of tumors through in situ biosynthesized fluorescent gold nanoclusters. *Sci. Rep.* **3**, 1157–1162 (2013).
21. H. Chang *et al*., Layer-by-layer assembly of graphene, Au and poly(toluidine blue O) films sensor for evaluation of oxidative stress of tumor cells elicited by hydrogen peroxide. *Biosens. Bioelectron.* **41**, 789–794 (2013).
22. H. Jiang, Y. Zhang, X. Wang, Single cytidine units-templated syntheses of multi-colored water-soluble Au nanoclusters. *Nanoscale* **6**, 10355–10362 (2014).
23. T. P. Szatrowski, C. F. Nathan, Production of large amounts of hydrogen peroxide by human tumor cells. *Cancer Res.* **51**, 794–798 (1991).
24. Y. C. Cao, R. Jin, C. A. Mirkin, Nanoparticles with Raman spectroscopic fingerprints for DNA and RNA detection. *Science* **297**, 1536–1540 (2002).
25. R. E. Dickerson, H. R. Drew, Kinematic model for B-DNA. *Proc. Natl. Acad. Sci. U.S.A.* **78**, 7318–7322 (1981).
26. D. K. Jangir, R. Mehrotra, Raman spectroscopic evaluation of DNA adducts of a platinum containing anticancer drug. *Spectrochim. Acta A Mol. Biomol. Spectrosc.* **130**, 386–389 (2014).
27. K. A. H. K. Katrin, Surface-enhanced Raman scattering and biophysics. *J. Phys. Condens. Matter* **14**, R597–R624 (2002).
28. K. Kneipp, H. Kneipp, I. Itzkan, R. R. Dasari, M. S. Feld, Ultrasensitive chemical analysis by Raman spectroscopy. *Chem. Rev.* **99**, 2957–2976 (1999).
29. B. Bin *et al*., Targeting CSCs in tumor microenvironment: The potential role of ROS-associated miRNAs in tumor aggressiveness. *Curr. Stem Cell Res. Ther.* **9**, 22–35 (2014).
30. Q. Feng *et al*., Hypoxia-specific therapeutic agents delivery nanotheranostics: A sequential strategy for ultrasound mediated on-demand tritherapies and imaging of cancer. *J. Control. Release* **275**, 192–200 (2018).
31. G. Widera *et al*., Increased DNA vaccine delivery and immunogenicity by electroporation in vivo. *J. Immunol.* **164**, 4635–4640 (2000).
32. M. E. Davis, Z. G. Chen, D. M. Shin, Nanoparticle therapeutics: An emerging treatment modality for cancer. *Nat. Rev. Drug Discov.* **7**, 771–782 (2008).
33. R. Khandelia, S. Bhandari, U. N. Pan, S. S. Ghosh, A. Chattopadhyay, Gold nanocluster embedded albumin nanoparticles for two-photon imaging of cancer cells accompanying drug delivery. *Small* **11**, 4075–4081 (2015).
34. A. K. Sahoo *et al*., Silver nanocluster embedded composite nanoparticles for targeted prodrug delivery in cancer theranostics. *ACS Biomater. Sci. Eng.* **2**, 1395–1402 (2016).
35. S. George *et al*., Loss of PTEN is associated with resistance to anti-PD-1 checkpoint blockade therapy in metastatic uterine leiomyosarcoma. *Immunity* **46**, 197–204 (2017).
36. H. Pan *et al*., Overexpression of circular RNA ciRS-7 abrogates the tumor suppressive effect of miR-7 on gastric cancer via PTEN/PI3K/AKT signaling pathway. *J. Cell. Biochem.* **119**, 440–446 (2018).
37. R. Mittler *et al*., ROS signaling: The new wave? *Trends Plant Sci.* **16**, 300–309 (2011).
38. H. Pelicano, D. Carney, P. Huang, ROS stress in cancer cells and therapeutic implications. *Drug Resist. Updat.* **7**, 97–110 (2004).
39. H. U. Simon, A. Haj-Yehia, F. Levi-Schaffer, Role of reactive oxygen species (ROS) in apoptosis induction. *Apoptosis* **5**, 415–418 (2000).
40. E. Sadauskas *et al*., Kupffer cells are central in the removal of nanoparticles from the organism. *Part. Fibre Toxicol.* **4**, 10–16 (2007).
41. H. S. Choi *et al*., Renal clearance of quantum dots. *Nat. Biotechnol.* **25**, 1165–1170 (2007).
42. M. Liu *et al*., Allele-specific imbalance of oxidative stress-induced growth inhibitor 1 associates with progression of hepatocellular carcinoma. *Gastroenterology* **146**, 1084–1096 (2014).
43. B. Sharif-Askari, L. Amrein, R. Aloyz, L. Panasci, PARP3 inhibitors ME0328 and olaparib potentiate vinorelbine sensitization in breast cancer cell lines. *Breast Cancer Res. Treat.* **172**, 23–32 (2018).
44. Q. Wang *et al*., SAMD9L inactivation promotes cell proliferation via facilitating G1-S transition in hepatitis B virus-associated hepatocellular carcinoma. *Int. J. Biol. Sci.* **10**, 807–816 (2014).
45. M. AlHarbi *et al*., Rare *TP53* variant associated with Li-Fraumeni syndrome exhibits variable penetrance in a Saudi family. *NPJ Genom. Med.* **3**, 35–40 (2018).
46. T. Kukolj *et al*., IL-33 guides osteogenesis and increases proliferation and pluripotency marker expression in dental stem cells. *Cell Prolif.* **52**, e12533 (2019).
47. M. Aman *et al*., Expression of protease-activated receptor-2 (PAR-2) is related to advanced clinical stage and adverse prognosis in ovarian clear cell carcinoma. *Hum. Pathol.* **64**, 156–163 (2017).
48. D. Liu *et al*., Genetic polymorphisms (rs10636 and rs28366003) in metallothionein 2A increase breast cancer risk in Chinese Han population. *Aging (Albany N.Y.)* **9**, 547–555 (2017).
49. E. Shoshan *et al*., NFAT1 directly regulates IL-8 and MMP-3 to promote melanoma tumor growth and metastasis. *Cancer Res.* **76**, 3145–3155 (2016).
50. Y. Wang *et al*., STX2 promotes colorectal cancer metastasis through a positive feedback loop that activates the NF-κB pathway. *Cell Death Dis.* **9**, 664–677 (2018).